Available online at www.sciencedirect.com
SCIENCE DIRECT
Carbon 44 (2006) 1826–1832
CARBON
www.elsevier.com/locate/carbon

Structure and mechanical properties of W incorporated diamond-like carbon films prepared by a hybrid ion beam deposition technique

Ai-Ying Wang [a], Kwang-Ryeol Lee [a,*], Jae-Pyoung Ahn [b], Jun Hee Han [c]

[a] Future Technology Research Division, Korea Institute of Science and Technology, P.O. Box 131, Cheongryang, Seoul, 130-650, South Korea
[b] Nano-Materials Research Center, Korea Institute of Science and Technology, Seoul, South Korea
[c] Materials Evaluation Center, Korea Research Institute of Standard Science, Yusung, South Korea

Received 24 March 2005; accepted 19 December 2005
Available online 21 February 2006

Abstract

W incorporated diamond-like carbon films were prepared on silicon(100) wafers using a hybrid deposition system composed of an end-Hall-type hydrocarbon ion gun and a tungsten DC magnetron sputter source. The W concentration in the films was controlled by changing the fraction of Ar in the Ar and C_6H_6 reaction gas. The chemical composition, atomic bond structure, and mechanical properties were investigated for W concentrations ranging from 0 to 8.6 at.%. When the W concentration was <2.8 at.%, the W atoms were dissolved in the amorphous carbon matrix without forming a WC_{1-x} phase. Amorphous and crystalline WC_{1-x} nano-particles appeared when the W concentration was >2.8 and >3.6 at.%, respectively. It was found that the hardness and elastic modulus were not sensitive to the W concentration in this concentration range. On the other hand, the residual compressive stress was strongly dependent on the chemical state of the incorporated W atoms. The change in mechanical properties is discussed in terms of the microstructural changes induced by W incorporation.

Keywords: Diamond-like carbon; Plasma deposition; Doping; Crystallite size; Mechanical properties

1. Introduction

Diamond-like carbon (DLC) films have been widely investigated owing to their unique properties, such as their high hardness values, wear resistance, chemical inertness, and low coefficient of friction. All of these properties make DLC coatings a strong candidate for sliding machine components or cutting tools [1–3]. However, high residual compressive stress of up to 10 GPa and low adhesion strength (especially with ferrous substrates) limits their practical application [4]. Recently, control of the substrate bias during deposition [5,6] or thermal annealing after deposition [7] has been used to manipulate the residual compressive stress of DLC coatings. However, addition of a third element, such as Al, Ni, Si, Fe, Ti, W, Cu, or Ag, has been the most common strategy used to control the residual compressive stress and improve adhesion and tribological properties of DLC coatings [8–15]. For example, using the filtered vacuum arc deposition technique, Lee et al. [8] observed a significant reduction in the residual stress of tetrahedral amorphous carbon films when a small amount of Si (<1 at.%) was incorporated in the film. In the case of Ti being incorporated into hydrogenated amorphous carbon (a-C:H) films, Meng and co-workers proposed that the residual stress gradually decreased as the percolation transition from an a-C:H phase to a TiC-like phase progress [9,10]. Metal-incorporated carbon composite films also exhibit many attractive characteristics. A very low coefficient of friction of <0.1 was reported in

* Corresponding author. Tel.: +82 2 958 5494; fax: +82 2 958 5509.
E-mail address: krlee@kist.re.kr (K.-R. Lee).

0008-6223/$ - see front matter © 2006 Elsevier Ltd. All rights reserved.
doi:10.1016/j.carbon.2005.12.045

Ti-incorporated a-C:H films prepared using a closed field unbalanced magnetron sputtering technique and in Ta-incorporated a-C:H films prepared using radio frequency (RF) diode sputtering [14]. Furthermore, metal incorporation to these films improves their chemical compatibility with a metal substrate, resulting in better adhesion [15].

It is generally observed that metal-incorporated DLC (Me-DLC) films are composed of nano-sized carbide particles dispersed in an amorphous matrix. The structural, mechanical, and electrical properties of these films are strongly influenced by the concentration, distribution, and size of the nano-particles in the amorphous carbon matrix [8–16]. The role of the incorporated metallic element on the structure and the properties is not yet fully understood. It should be also noted that in most of the previously reported experimental work, the atomic bond structure of the carbon varied with metal incorporation, which made it difficult to understand the full effect of metal incorporation on the film properties.

In this work, we reported on the results of an in-depth analysis of the microstructure and atomic bond structure of W incorporated DLC (W-DLC) films prepared using a hybrid deposition method. The deposition method composed of a hydrocarbon ion beam and a tungsten DC magnetron sputterer, and enabled us to investigate the effect of W incorporation without invoking any structural change in the amorphous carbon matrix. We focused on the relationship between the mechanical properties and the microstructure of the films. It was observed that the residual compressive stress was strongly dependent on the state of the incorporated W atoms, whereas the mechanical properties were not sensitive to the concentration of the W, and thus to the state of the incorporated W atoms.

2. Experimental

A schematic diagram of the hybrid deposition system used in our work is shown in Fig. 1. The deposition method combined the ion beam deposition of benzene with the DC magnetron sputtering of tungsten. The C_6H_6 was introduced into the end-Hall-type ion gun to obtain the hydrocarbon ions. Typical value of anode voltage and current are 150 V and 0.48 A, respectively. Argon sputtering gas was supplied to the sputter gun equipped with a high purity (99.95%) W target of diameter 5 cm. Typical dc power supplied to the sputter gun was about 65 W (430 V, 0.15 A). The fraction of Ar in the reaction gas was varied from 0.50 to 0.95 to control the W concentration in the deposited films. The base pressure in the reactor was $<3\times10^{-4}$ Pa, whereas the deposition pressure varied in the range 0.08–0.15 Pa, depending on the fraction of Ar gas. Before deposition, the substrate was cleaned using the Ar-ion beam employing a pressure of 0.10 Pa and a bias voltage of −200 V for a period of 15 min. Subsequently, the sputter source was operated for a period of 20 min with the shutter closed to remove any surface poisoning of the W target. All the samples were deposited using a substrate

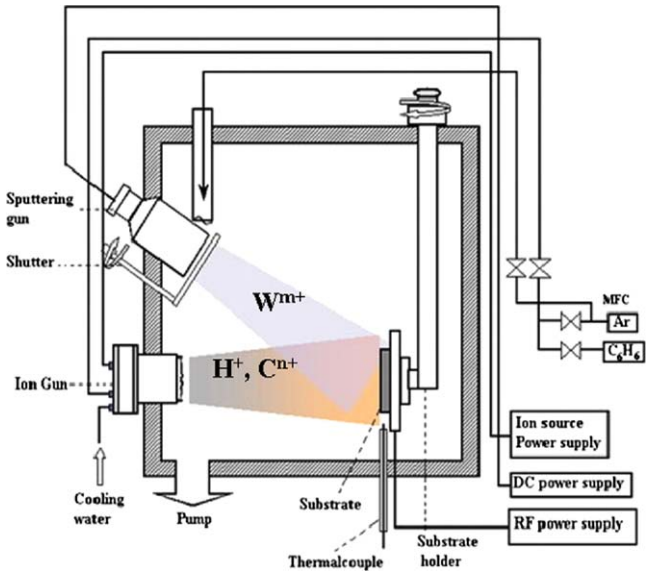

Fig. 1. Schematic diagram of the hybrid ion beam deposition system used.

bias of −200 V. Pure DLC films were also prepared using the hydrocarbon ion beam and a negative substrate bias of −200 V without operating the sputter gun. The deposition time was adjusted to obtain a film thickness of 300 ± 50 nm for all the samples.

A p-type Si(100) wafer with thickness 500 ± 10 μm was used for the substrate, and this was fixed on a rotating substrate holder placed about 22 cm from the ion gun. A thin Si(100) wafer of thickness 105 ± 5 μm was also used to estimate the residual stress from the observed curvature of the film/substrate composite [17]. The thickness of the deposited film was measured using an α-step profilometer employing a step made using a shadow mask. The composition of the film was analyzed using Rutherford backscattering spectrometry (RBS) and elastic recoil detection (ERD) analysis employing a 2-MeV collimated $^4He^{2+}$ ion beam. 2 MV Pelletron accelerator of National Electrostatic Corporation was used for the He ion acceleration. Homemade analysis chamber was used to collect the RBS and ERD spectra. A high-resolution transmission electron microscope (HRTEM) with a dedicated parallel electron energy loss spectroscopy (EELS) attachment was employed to characterize the microstructure and the chemical bond structure of the film, respectively. Plan-view samples were prepared using a mechanical and chemical polishing method to minimize any thermal effects on the microstructure. All the EELS spectra were acquired using a combination of a Tecnai G2 transmission electron microscope (FEI com) equipped with a field emission source (Schottky emitter) and a GIF2002 (Gatan Inc.) with an energy resolution of 0.7 eV. In the EELS experiments, the STEM mode with a spot size of 0.2 nm was employed, and the spectrometer was operated under fixed conditions, with an entrance aperture = 2.0 mm and a channel step size = 0.3 eV. The spatial resolution of the EELS was estimated to be <1 nm. Grazing incidence X-ray diffraction (GIXRD:

DMAX2500 manufactured by Rigaku Co.) with an incidence angle of 1° and micro-Raman spectroscopy (Lab-Ram HR manufactured by Jovin-Yvon) using a $\lambda = 514.5$ nm Ar-ion laser were also employed to characterize the atomic bond structure of the films. Nano Indenter II of Nano Instruments, Inc. was used for the hardness measurement. Nano-indentation in the continuous stiffness measurement (CSM) mode was employed to characterize the hardness and elastic modulus of the films. A characteristic hardness of the films was chosen as being the depth where the measured values were not affected by the mechanical properties of the substrate.

3. Results and discussion

Fig. 2 shows the dependence of the W concentration in the films on the fraction of Ar in the supply gas mixture. When the Ar fraction was <0.58, a W-incorporated film could not be obtained, due to the unstable operation of the magnetron sputter gun and significant poisoning of the target caused by the high flux of carbon ions. However, as the Ar fraction increased from 0.58 to 0.90, the W concentration monotonically increased from 1.9 to 8.6 at.%. This indicated that the W concentration in the film could be systematically controlled by varying the fraction of Ar in the reaction gas. A similar behavioral trend was reported using an radio frequency plasma assisted chemical vapor deposition (RF-PACVD) and DC magnetron sputtering hybrid deposition system [11]. When the Ar fraction was >0.90, the deposited films exhibited the characteristics of pure W films, with a typical metallic gloss. In our work, a small concentration of Ar (<2 at.%) was also observed in all the W incorporated films. The inset of Fig. 2 shows that the hydrogen concentration decreased monotonically from 33.7 to 30.2 at.% with increasing Ar fraction from 0.58 to 0.90. The growth rate of the film decreased from 28.5 to 15.1 nm/min as the Ar fraction increased. As the substrate was not cooled, the temperature of the substrate increased during deposition. However, the maximum temperature of the sample did not exceed 200 °C, as confirmed by a thermocouple placed in the vicinity of the substrate.

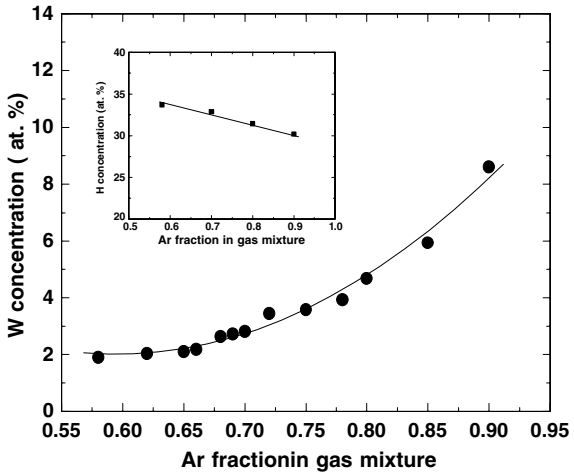

Fig. 2. Dependence of W concentration in the deposited film on the fraction of Ar in the reaction gas. Inset shows the representative H concentration in the film as a function of Ar fraction.

Fig. 3 shows high-resolution TEM microstructures and the corresponding selected area electron diffraction patterns for various W concentrations. At a W concentration of 1.9 at.% (Fig. 3(a)), only an amorphous granular structure with diffuse hallows in the diffraction pattern was observed. This microstructure is essentially the same as that of a pure a-C:H film, showing that all the incorporated W atoms were dissolved in the amorphous carbon matrix. As the W concentration increased, an amorphous WC_{1-x} phase began to evolve. At a W concentration of 2.8 at.%, localized dark regions with a diameter of ~1 nm appeared in the TEM microstructure, as indicated by the arrow in Fig. 3(b). These dark regions evolved into a crystalline WC_{1-x} phase as the W concentration increased. However, the corresponding electron diffraction patterns showed that the crystalline phase had yet to be evolved. WC_{1-x} crystallites appeared at W concentrations >3.6 at.%, where a noticeable diffraction ring was observed, as can be seen in Fig. 3(c). The degree of crystallinity and the size of the WC_{1-x} crystallites increased with further increases in W concentration. Fig. 3(d) shows that WC_{1-x} crystallites with a diameter of about 2 nm were dispersed in the amorphous carbon matrix at W concentrations of 8.6 at.%.

The electron diffraction patterns clearly show the formation of α-W_2C in the films. The TEM microstructures in Fig. 3 reveal three stages of structural evolution on W incorporation: The W atoms were dissolved in the a-C:H matrix when the W concentration was low (<2.8 at.% W). As the W concentration increased, the W atoms began to segregate to form an amorphous WC_{1-x} phase in the matrix. The WC_{1-x} phase eventually evolved into a nano-sized crystalline α-W_2C phase when the W concentration increased above 3.6 at.%. Fig. 4 shows high-resolution TEM microstructures of the tungsten carbide crystallites with a [0 1 1] zone axis along with the simulated SAD pattern. The microstructure shows that the crystal had a hexagonal close packed structure. The planar spacing of the (1 0 1) and (1 0 0) planes were 2.293 and 2.593 Å, respectively, which were attributed to the α-W_2C phase.

The structural changes on W incorporation were also confirmed by the GIXRD spectra. The GIXRD spectra of films having various W concentrations are summarized in Fig. 5. The intensity of the spectra was normalized to the film thickness, and shifted upward for ease of comparison. No significant diffraction peak was observed when the W concentration was <3.6 at.%. However, a broad diffraction peak at $2\theta = 37°$ began to appear at a W concentration of 3.6 at.%. A small peak at about $2\theta = 57°$ was observed when the W concentration was 1.9 at.%. The origin of this peak is not clear, but seems to be an artifact of the analysis equipment used in our work. As indicated by the simulation pattern shown in the bottom of Fig. 5, the crystalline α-W_2C phase should have a strong (1 0 1) diffraction peak

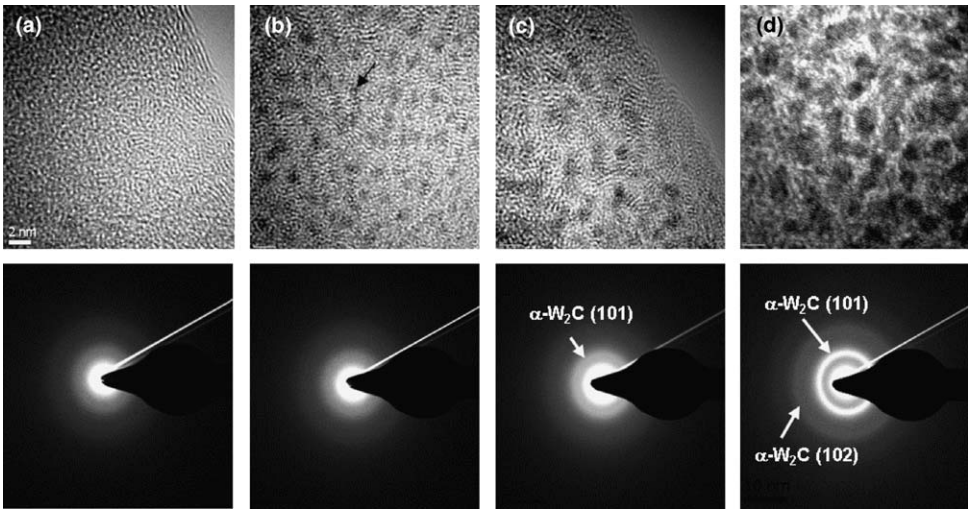

Fig. 3. High-resolution TEM images and selected area electron diffraction patterns of films with W concentrations of (a) 1.9 at.%, (b) 2.8 at.%, (c) 3.6 at.%, and (d) 8.6 at.%.

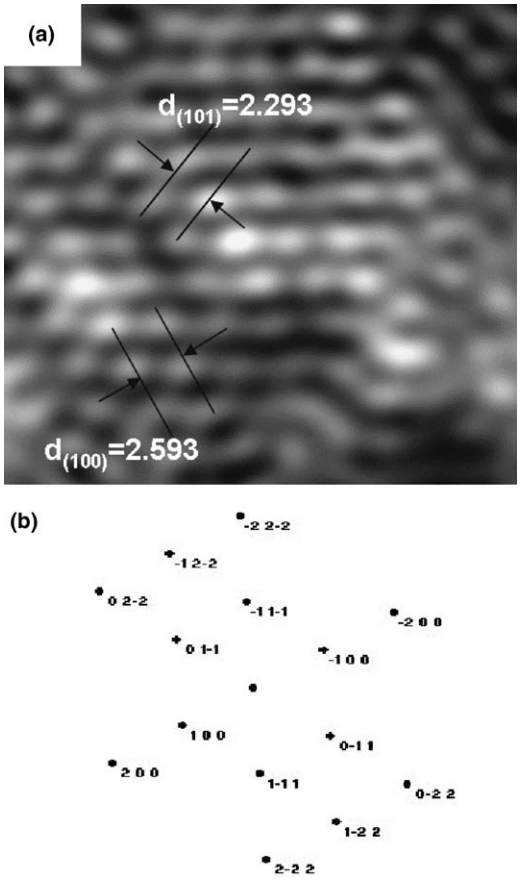

Fig. 4. HRTEM microstructure of W_2C nano-crystallites, and the simulated selected area diffraction pattern with 8.6 at.% W incorporation.

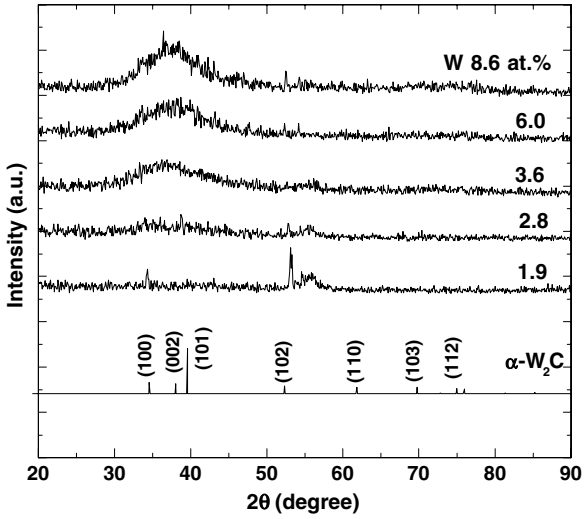

Fig. 5. Evolution of the grazing incidence XRD spectra of W incorporated DLC films as a function of W concentration.

at $2\theta = 39.569°$ with other various weak diffraction peaks. The broad peak near to $2\theta = 37°$ would correspond to this (1 0 1) diffraction peak. The downward shift of the peak may be the result of any residual compressive stress in the film. The intensity of the peak increased with increasing W concentration, indicating that the crystallinity of the carbide phase increased as the W concentration increased.

Even though the evolution of the WC_{1-x} phase appeared to be strongly dependent on the W concentration, the structure of the a-C:H matrix was not influenced by W incorporation. Fig. 6(a) shows high-resolution carbon K-edge EELS spectra of the matrix. Since the spatial resolution of the EELS spectra was <1 nm, the EELS spectra only represent the atomic bond structure of the matrix. The spectra were normalized with respect to the σ^* peak and are vertically shifted for ease of comparison. The spectrum shows a peak near to 286 eV, which is associated with the transition from the C 1s state to the empty π^* state of the sp^2 sites. (In our experiments, where high kinetic energy ions bombard the surface during growth, the number of sp^1 hybridized bonds would be negligible.) The large, broad peak observed at about 295 eV is due to the transition to

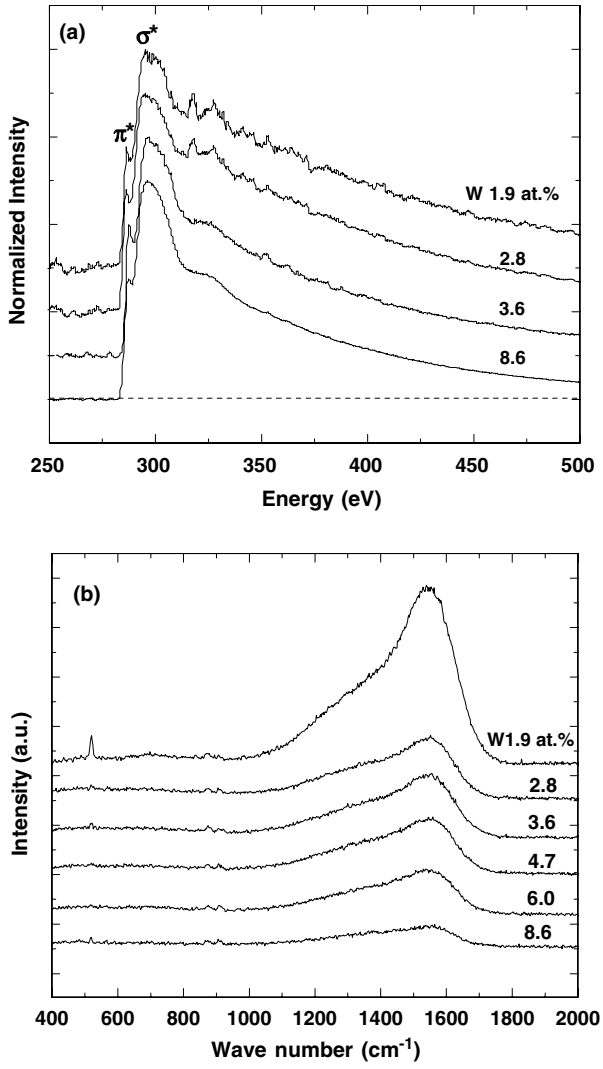

Fig. 6. (a) Carbon K-edge EELS spectra and (b) micro-Raman spectra for W incorporated DLC films with various W concentrations.

the empty σ^* state of both the sp^3 and sp^2 sites. Hence, the ratio of these two peaks has been used to characterize the atomic bond structure of amorphous carbon materials [18,19]. The ratio of the intensities of the π^* and σ^* peaks was 0.55 ± 0.1 regardless of the W concentration. This result suggests that the ratio of the sp^2 to sp^3 hybridized bonds does not vary with W incorporation. When the W concentration was <3.6 at.%, unidentified small peaks near to 317 and 327 eV appeared. These peaks disappeared when the nano-crystalline WC_{1-x} particles were formed in the film, which suggests that these peaks correspond to W–C bonds in the amorphous carbon matrix.

Fig. 6(b) shows the Raman spectra observed for various W concentrations. On increasing the W concentration, the peak intensity decreased markedly, because of the increasing fraction of a centrosymmetric phase, such as WC_{1-x}, which is inactive to Raman excitation. This result showed that a centrosymmetric phase began to form when the W concentration was >1.9 at.%. The carbon Raman peak could be deconvoluted into the D and G peaks, and the G-peak position of a film can be used to observe the structural variations in the film [20]. It is known empirically that the G-peak position of a Raman spectrum shifts to a higher wavenumbers as the graphitic component in the film increases. The G-peak position in our films varied over a small range from 1554.5 to 1557.8 cm^{-1} when the W concentration increased from 1.9 to 8.6 at.%. Therefore, both the EELS and Raman spectroscopy analyses show that the atomic bond structure of the carbon network was not changed on W incorporation.

Fig. 7 shows the compressive residual stress (Fig. 7(a)) and mechanical properties (Fig. 7(b)) of the films as a function of W concentration. The residual stress exhibited an unusual behavior with increasing W concentration up to 8.6 at.%. As the W concentration increased from 0 to 2.8 at.%, the residual stress decreased monotonically from 2.9 to 1.5 GPa. Comparing this result with the structural analysis, we note that the decrease in the residual stress in this concentration range is accompanied with the W

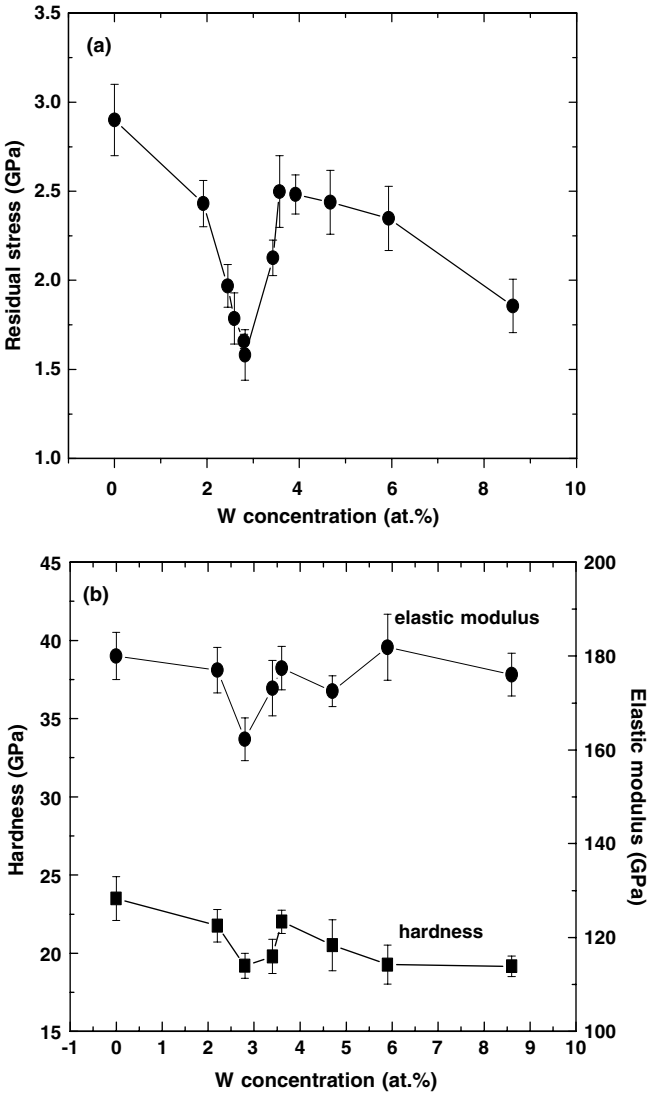

Fig. 7. (a) Residual compressive stress and (b) mechanical properties of W incorporated DLC films as a function of W concentration.

dissolution into the amorphous carbon matrix without forming a carbide phase. In previous work, we suggested that W atoms in an amorphous carbon matrix play the role of a pivotal site, whereby distortion of the atomic bond angles can occur without inducing a significant increase in the elastic energy [21]. Further incorporation of W up to 3.6 at.% rapidly increased the residual compressive stress to 2.5 GPa. This increase is concurrent with the formation of an amorphous WC_{1-x} phase in the matrix. The W–C bond length is longer than the C–C bond length, and this would play a significant role in this composition range. When the W concentration increased from 3.6 to 8.6 at.%, the residual stress gradually decreased to 1.8 GPa, which correlates with the evolution of the crystalline α-W_2C phase. Such a gradual decrease in residual stress at higher W concentrations can be understood by the percolation structural transition from an a-C:H rich structure to a WC_{1-x} rich structure [9,10,13,22–24].

The mechanical properties exhibited a similar dependence on the W concentration, as shown in Fig. 7(b). However, it must be noted that the change in the mechanical properties was not as significant as that seen in the residual stress. The hardness and elastic modulus were estimated to be 21 ± 3 and 175 ± 15 GPa, respectively, regardless of the W concentration. Analysis of the atomic bond structure (Fig. 6) shows that the three-dimensional interlinkage of the atomic bond network in the carbon matrix does not vary with W concentration. Therefore, the mechanical properties of the film were mainly attributable to those of the amorphous carbon matrix rather than those of the carbide crystallites. This result can be understood if one considers that each carbide particle is isolated in the amorphous carbon matrix in the concentration range studied.

4. Conclusions

A hybrid ion beam deposition system incorporating an end-Hall-type ion gun and DC magnetron sputtering has been successfully employed to deposit W incorporated DLC films. The W concentration of the films could be varied from 1.9 to 8.6 at.% by changing the fraction of Ar gas in a mixture of Ar and C_6H_6. The films were composed of WC_{1-x} nano-particles and a hydrogenated amorphous carbon matrix. The most significant result is that the W atoms were incorporated without changing the atomic bond structure of the amorphous carbon matrix. Therefore, the experimental conditions used provide the opportunity to investigate an indisputable effect of W incorporation on the microstructure and properties of deposited films. The mechanical properties are mainly governed by the three-dimensional interlinkage of the carbon network, and this was not degraded by W incorporation. On the other hand, the residual compressive stress is strongly dependent on the state of the incorporated W atoms. When the W atoms were dissolved in the amorphous carbon matrix, the pivotal action of the W atoms reduces the strain energy arising from the distortion of the bond angles, resulting in a significant reduction of the residual stress. However, segregation of the W atoms increases the residual stress significantly. At higher W concentrations, nano-sized WC_{1-x} crystallites evolved, resulting in a gradual decrease in the residual compressive stress. Our work shows the possibility of fabricating films with a reduced residual stress, without observing any associated degradation of the mechanical properties.

Acknowledgements

This research was financially supported by the Ministry of Science and Technology of Korea through the International Cooperation Research Program.

References

[1] Lee KR, Eun KY. Tribology of diamond-like carbon coated VCR head drums. Mater Sci Eng A 1996;209:264–9.
[2] Voevodin AA, Zabinski JS. Superhard, functionally gradient, nanolayered and nanocomposite diamond-like carbon coatings for wear protection. Diamond Relat Mater 1998;7:463–7.
[3] Hauert R, Patscheider J. From alloying to nanocomposites-improved performance of hard coatings. Adv Eng Mater 2000;2:247–59.
[4] Zhang SL, Johnson HT, Wagner GJ, Liu WK, Hsia KJ. Stress generation mechanisms in carbon thin films grown by ion-beam deposition. Acta Mater 2003;51:5211–22.
[5] Pharr GM, Callahan DL, McAdams SD, Tsui TY, Anders S, Anders A, et al. Hardness, elastic modulus, and structure of very hard carbon films produced by cathodic-arc deposition with substrate pulse biasing. Appl Phys Lett 1996;68:779–81.
[6] Kumar S, Dixit PN, Sarangi D, Bhattacharyya R. Possible solution to the problem of high built-up stresses in diamond-like carbon films. J Appl Phys 1999;85:3866–77.
[7] Friedmann TA, Sullivan JP, Knapp JA, Tallant DR, Follstaedt DM, Medlin DL, et al. Thick stress-free amorphous-tetrahedral carbon films with hardness near that of diamond. Appl Phys Lett 1997;71:3820–2.
[8] Lee CS, Lee KR, Eun KY, Yoon KH, Han JH. Structure and properties of Si incorporated tetrahedral amorphous carbon films prepared by hybrid filtered vacuum arc process. Diamond Relat Mater 2002;119:198–203.
[9] Shi B, Meng WJ, Rehn LE, Baldo PM. Intrinsic stress development in Ti–C:H ceramic nanocomposite coatings. Appl Phys Lett 2002;81:352–4.
[10] Shi B, Meng WJ. Intrinsic stresses and mechanical properties of Ti-containing hydrocarbon coatings. J Appl Phys 2003;94:186–94.
[11] Park SJ, Lee KR, Ko DH, Eun KY. Microstructure and mechanical properties of WC–C nanocomposite films. Diamond Relat Mater 2002;11:1747–52.
[12] Zhang P, Tay BK, Sun CQ, Lau SP. Microstructure and mechanical properties of nanocomposite amorphous carbon films. J Vac Sci Technol A 2002;20:1390–4.
[13] Fryda M, Taube K, Klages CP. Nanometer indentation measurements on metal-containing amorphous hydrogenated carbon films. Vacuum 1990;41:1291–3.
[14] Pauleau Y, Thiery F. Deposition and characterization of nanostructured metal/carbon composite films. Surf Coat Technol 2004;180–181:313–22.
[15] Okpalugo TIT, Maguire PD, Ogwu AA, McLaughlin JAD. The effect of silicon doping and thermal annealing on the electrical and structural properties of hydrogenated amorphous carbon thin films. Diamond Relat Mater 2004;13:1549–52.
[16] Zhang S, Sun D, Fu YQ, Du HJ. Recent advances of superhard nanocomposite coatings: a review. Surf Coat Technol 2003;167:113–9.

[17] Ohring M. The materials science of thin films. New York: Harcourt Brace Jovanovich; 1991, p. 416–8.
[18] Fallon PJ, Veerasamy VS, Davis CA, Robertson J, Amearatunga GAJ, Milne WI, et al. Properties of filtered-ion-beam-deposited diamondlike carbon as a function of ion energy. Phys Rev B 1993;48:4777–82.
[19] Robertson J. Electronic and atomic structure of diamond-like carbon. Semicond Sci Technol 2003;18:S12–9.
[20] Shin JK, Lee CS, Lee KR, Eun KY. Effect of residual stress on the Raman spectrum analysis of tetrahedral amorphous carbon films. Appl Phys Lett 2001;27:631–3.
[21] Wang AY, Ahn HS, Lee KR, Ahn JP. Unusual stress behavior in W-incorporated hydrogenated amorphous carbon films. Appl Phys Lett 2005;86:111902.
[22] Meng WJ, Gillispie BA. Mechanical properties of Ti-containing and W-containing diamond-like carbon coatings. J Appl Phys 1998; 84:4314–21.
[23] Feng B, Cao DM, Meng WJ, Rehn LE, Baldo PM, Doll GL. Probing for mechanical and tribological anomalies in the TiC/amorphous hydrocarbon nanocomposite coating system. Thin Solid Films 2001;398–399:210–6.
[24] Klages CP, Köberle H, Bauer M, Memming R. Properties and microstructure of metal-containing a-C:H films. Proceedings of the first international symposium on diamond and diamond-like films. Los Angeles (CA), USA: The Electrochemical Society; 1989, p. 225–36.